HHS Public Access

Author manuscript

Oncogene. Author manuscript; available in PMC 2021 April 06.

Published in final edited form as:

Oncogene. 2020 December ; 39(49): 7153–7165. doi:10.1038/s41388-020-01489-4.

The V654A second-site *KIT* mutation increases tumor oncogenesis and STAT activation in a mouse model of gastrointestinal stromal tumor

Jennifer Q. Zhang[1,#], **Benedikt Bosbach**[2,3,#], **Jennifer K. Loo**[1], **Gerardo A. Vitiello**[1], **Shan Zeng**[1], **Adrian M. Seifert**[1], **Benjamin D. Medina**[1], **Nesteene J. Param**[1], **Joanna H. Maltbaek**[1], **Ferdinand Rossi**[1,5], **Cristina R. Antonescu**[4], **Peter Besmer**[2,#], **Ronald P. DeMatteo**[1,5,#,*]

[1]Department of Surgery, Memorial Sloan Kettering Cancer Center, New York, NY

[2]Department of Developmental Biology, Memorial Sloan Kettering Cancer Center, New York, NY

[3]Department of Cancer Biology and Genetics,Memorial Sloan Kettering Cancer Center, New York, NY

[4]Department of Pathology, Memorial Sloan Kettering Cancer Center, New York, NY,

[5]Department of Surgery, Hospital of the University of Pennsylvania, Philadelphia, PA

Abstract

Gastrointestinal stromal tumor (GIST) is the most common human sarcoma and arises in the gastrointestinal tract. Most GISTs are caused by activating mutations in the KIT receptor tyrosine kinase, such as the exon 11 *KIT* V559Δ mutation. The small molecule imatinib inhibits KIT and has been a mainstay of therapy in GIST. Unfortunately, imatinib-treated patients typically relapse, most often due to clonal emergence of the resistance-associated *KIT* V654A mutation. To determine the biologic impact of this second-site mutation *in vivo*, we created a mouse model with the corresponding V558Δ;V653A *Kit* double mutation restricted (a) spatially to ETV1^{+} cells, which include the interstitial cells of Cajal (ICCs) from which GISTs presumably originate, and (b) temporally through tamoxifen treatment after birth. This resulted in the first *in vivo* model of the most common second-site mutation associated with imatinib resistance in GIST and the first *in vivo* demonstration that cell-autonomous expression of mutant KIT in the ICC lineage leads to GIST. GISTs driven by the V558Δ;V653A *Kit* double mutation were resistant to imatinib, while cabozantinib was more effective in overcoming resistance than sunitinib. Compared to control mice with a single V558Δ *Kit* mutation, mice with a double V558Δ;V653A *Kit* mutation had increased tumor oncogenesis and associated KIT-dependent STAT activation. Our findings demonstrate that the biologic consequences of a second-site mutation in an oncogenic driver may

[*]**Corresponding author**: Ronald P. DeMatteo MD, Hospital of the University of Pennsylvania, Philadelphia, PA 19104, Phone: 215-662-7539, Fax: 215-614-0363, ronald.dematteo@pennmedicine.upenn.edu.
[#]Contributed equally to the manuscript

Conflict of interest statement. BB is an employee of Pfizer and holds shares in the company. RPD is the recipient of a grant from Blueprint Medicines for an unrelated study. Neither affiliation is related to the contents of this study. Remainder of the authors declare no conflicts of interest.

include not only a mechanism for drug resistance, but changes in tumor oncogenic potential and differential activation of signaling pathways.

Keywords

Gastrointestinal stromal tumor; V654A; *Kit* mutation; imatinib resistance; STAT activation

Introduction

The development of tyrosine kinase inhibitors has revolutionized the treatment of multiple malignancies that are primarily driven by a particular oncogene. Gastrointestinal stromal tumors (GISTs), a common sarcoma occurring primarily in the stomach and small intestine, are thought to arise from the interstitial cells of Cajal and are characterized by activating mutations in *KIT* in 75% of cases or platelet derived growth factor receptor alpha (*PDGFRA)* in 10% of cases[1, 2]. Imatinib mesylate, an inhibitor of KIT, ABL1, and PDGFRA, has improved survival of patients with GIST[3–5]. However, resistance to imatinib is a major hurdle to cure, as it commonly develops within two years[3, 6]. Acquired resistance to imatinib is typically due to manifestation of clones with a second-site mutation in *KIT*[7]. The most frequent acquired *KIT* mutation in GIST is V654A in exon 13[8–10]. The mutation occurs in the ATP binding pocket of the kinase domain and inhibits binding of imatinib[9]. This imatinib-resistant mutation can be overcome with sunitinib[11, 12], but usually only for a few months[13].

Our previous germline mouse model of GIST containing a *Kit* exon 11 (V558Δ) mutation resulted in tumors that were 100% penetrant, histologically indistinguishable from human GIST, and responsive to imatinib therapy[14]. This model has been used in the discovery of multiple new targeted therapies such as pexidartinib and cabozantinib[15, 16], the role of ETV1 in GIST tumorigenesis[17, 18], and the contribution of the immune environment during imatinib therapy[19–22]. While GIST cell lines and patient-derived xenografts with primary and second-site *KIT* mutations exist, they are heterogeneous and have accumulated other genetic defects and are typically grown in immunodeficient mice, thereby potentially obscuring the additional effects of the second-site *KIT* mutation. Therefore, we sought to create a genetically engineered GIST mouse model with a common primary *KIT* mutation plus the most frequently acquired second-site *KIT* mutation. Such a model might reveal how the addition of the V654A mutation alters tumor cell biology, KIT signaling, and the tumor microenvironment, and would allow new treatments to be tested.

Results

Germline $Kit^{V558\Delta;V653A/+}$ mice exhibit perinatal lethality.

According to the Catalogue of Somatic Mutations in Cancer database (COSMIC), the most common second-site *KIT* mutation in human GIST is V654A, which corresponds to mouse V653A (Fig. 1A). We sought to create a germline mouse model of a V558Δ;V653A *Kit* double mutation (Fig. 1B) in order to further delineate the *in vivo* effects of the additional V653A mutation and study potential therapies. Although germline V558Δ *Kit* single mutant

mice are viable[14], the V558Δ;V653A *Kit* double mutant conferred perinatal lethality, with no mice surviving past the day of birth (Fig. 1C). We hypothesized that the death of the germline double mutant was due to increased KIT signaling leading to transformation in the hematopoietic lineage, given our previous findings that *Kit* mutations can lead to blood dyscrasias[23] and our observation that V558Δ;V653A newborns were bright red. The vav-Cre system allows for gene expression to be restricted to the hematopoietic lineage[24]. By breeding $Kit^{V558\Delta;V653A\text{-}NEO/+}$ mice to vav-Cre mice, we showed that the presence of the double mutation in hematopoietic cells alone was sufficient to result in perinatal lethality (Fig. 1D), suggesting increased aggressiveness of the V558Δ;V653A *Kit* mutation compared to the V558Δ *Kit* single mutant in the hematopoietic system.

Inducible lineage-specific $Kit^{V558\Delta;V653A\text{-}NEO/+}$; $Etv1^{Cre\text{-}ERT2/+}$ mice develop intestinal GIST.

To create a viable mouse model containing the V653A second-site mutation, we utilized the $Etv1^{Cre\text{-}ERT2/+}$ mouse, as ETV1 was previously identified as a lineage-specific transcription factor required for GIST development[17, 18]. $Rosa26^{floxSTOP\text{-}tdTomato}$ mice were crossed to $Etv1^{Cre\text{-}ERT2/+}$ mice and progeny were injected at birth with tamoxifen and sacrificed at 8 weeks of age. IHC staining for tdTomato, indicating presence of ETV1 expression, was present in a pattern typical for myenteric and intramuscular ICCs[25] in the stomach, cecum, and colon of tamoxifen-induced mice (Fig. 2A). In order to induce the selective expression of the V558Δ;V653A *Kit* double mutation in ETV1-expressing cells, $Kit^{V558\Delta;V653A\text{-}NEO/+}$ mice were crossed to $Etv1^{Cre\text{-}ERT2/+}$ mice and treated at birth with tamoxifen. Mice developed cecal GIST (Fig. 2B), which appeared histologically similar to human GIST on H&E staining and expressed both KIT and the GIST marker DOG1[26] (Fig. 2C). For simplicity, $Kit^{V558\Delta;V653A\text{-}NEO/+}$; $Etv1^{Cre\text{-}ERT2/+}$ mice induced with tamoxifen at birth will be referred to as V558Δ;V653A mice. Tumor weight increased with age (Fig. 2D) and tumor weight at 5 months did not depend on the timing of tamoxifen injection within the first 5 days after birth (Fig. 2E). Since the *Kit* mutant allele was only fully activated in ETV1-expressing cells and represented a hypomorphic allele in ETV1-negative cells, which did not undergo excision of the floxed NEO cassette, there was reduced KIT expression in cells that do not express ETV1, such as melanocytes. As described for heterozygous loss-of-function *Kit*[27], we observed white paws, tail tips, and belly spots in $Kit^{V558\Delta;V653A\text{-}NEO/+}$ mice, independent of the $Etv1^{Cre\text{-}ERT2/+}$ allele and tamoxifen induction, likely resulting from altered melanocyte migration during development (Supplemental Fig. 1A). There were minimal differences in hemoglobin, mean corpuscular volume (MCV), platelets, and white blood cell count (WBC) in V558Δ;V653A mice compared to WT and V558Δ mice (Supplemental Fig. 1B).

The V653A second-site mutation leads to increased oncogenesis compared to the V558Δ single mutation.

To serve as a comparison for the V558Δ;V653A double mutant mouse model, an inducible model of the V558Δ single *Kit* mutation was created by breeding $Kit^{V558\Delta\text{-}NEO/+}$ mice to $Etv1^{Cre\text{-}ERT2/+}$ mice (Fig. 3A) and injecting the progeny with tamoxifen between days 0 and 5 after birth. We will refer to the $Kit^{V558\Delta\text{-}NEO/+}$; $Etv1^{Cre\text{-}ERT2/+}$ mice induced at birth with tamoxifen as V558Δ mice. V558Δ mice also developed cecal GISTs. While histologic appearance of the two tumors was similar, there was increased ICC hyperplasia in the colon

and stomach of V558Δ;V653A mice compared to V558Δ mice (Fig. 3B). In addition, at 5 months the tumors of V558Δ;V653A mice had increased tumor weight compared to tumors of V558Δ mice (Fig. 3C). V558Δ;V653A mice also had decreased body weight (Fig. 3C) and decreased survival (Fig. 3D). V558Δ;V653A tumors had increased proliferation as indicated by higher Ki67 by IHC (Fig. 3E) and higher Ki67 of KIT^+ tumor cells on flow cytometry (Fig. 3F). Because mouse GISTs do not grow well *in vitro*, in order to delineate the effect of the V653A second-site mutation on cell growth independent of the tumor environment, we derived mast cells (which express KIT) with the V558Δ;V653A double mutation. V558Δ;V653A mast cells had increased proliferation both with and without IL-3 (which is usually required for mast cell growth) in culture over one week when compared to V558Δ and WT mast cells (Fig. 3G). These data point to the increased oncogenic potential conferred by the addition of the V653A mutation.

Cabozantinib demonstrates greater efficacy than sunitinib in imatinib-resistant V558Δ;V653A GISTs.

After treatment of V558Δ;V653A mice with imatinib (45 mg/kg i.p.) for one week, there was no effect on phosphorylation of KIT or its downstream mediators (Fig. 4A). It was previously reported that high doses of imatinib at 3μM or greater had the ability to inhibit phosphorylation of the V654A KIT mutant *in vitro*[10]. We therefore treated V558Δ;V653A mice with high-dose imatinib (90 mg/kg i.p.) and harvested tumors at 6 hours. There was no inhibition of p-KIT Y719 (Fig. 4B) with high dose imatinib treatment *in vivo*. Given some suggestion that imatinib leads to clinical stabilization in human GISTs with the V654A second-site mutation[28], serial MRI was performed to assess tumor volume at 1 and 4 weeks of imatinib treatment. Unlike the 50–75% reduction in tumor size that we have shown in $Kit^{V558/+}$ mice at 1 week[19, 21], imatinib did not decrease tumor volume in V558Δ;V653A mice but did stabilize growth (Fig. 4C). This is suggestive of a minor off-target, KIT-independent effect of imatinib therapy.

Sunitinib is currently the first-line treatment for V654A *KIT* mutant GISTs. As expected, 1 week of sunitinib was effective at inhibiting p-KIT and downstream signaling in V558Δ;V653A GISTs (Fig. 4D). There was increased collagen deposition on Trichrome staining and decreased proliferation as measured by Ki67 staining (Fig. 4E, F). Given our previous study demonstrating dramatic *in vivo* tumor inhibition with cabozantinib[15], as well as a previous report of *in vitro* inhibition of the V654A KIT mutation[29], we hypothesized cabozantinib would be superior to the current standard of care treatment sunitinib in our *in vivo* V558Δ;V653A model. Indeed, cabozantinib had an even more profound effect on V558Δ;V653A tumors compared to sunitinib and resulted in decreased cellularity on H&E, increased collagen deposition on Trichrome, and less Ki67 staining (Fig. 4E, F). Of note, we and others have used trichrome staining as an indicator of tumor response[16, 18, 22]. Western blot of V558Δ;V653A tumors treated with cabozantinib for 1 week demonstrated dramatically decreased total KIT (Fig. 4G), likely due to significant tumor death.

The V653A second-site mutation increases KIT-dependent STAT signaling.

Given the increased tumor growth conferred by the V653A second-site mutation, we sought to determine the changes in signaling. Surprisingly, there were no differences in p-KIT Y719 (Fig. 5A–B) or in total KIT phospho-tyrosine levels (Fig. 5B). We investigated various downstream pathways as a readout of KIT activity, including MAPK, PI3K, and STAT signaling, based on previous studies[30–32]. Although no differences were seen in MAPK or PI3K pathway activation (Fig. 5A), p-STAT3 and p-STAT5 signaling was increased in V558Δ;V653A tumors (Fig. 5C). Given previous description of direct interaction of STATs with KIT[32], we performed immunoprecipitation of STAT3 and STAT5, which demonstrated increased co-immunoprecipitation with KIT in V558Δ;V653A tumors (Fig. 5D **left**). To verify our results, we performed immunoprecipitation of KIT, which demonstrated increased co-immunoprecipitation with STAT3 and STAT5 (Fig. 5D **center and right**). Imatinib did not inhibit p-KIT, p-STAT3, or p-STAT5 in V558Δ;V653A tumors (Fig. 5E), while sunitinib and cabozantinib appeared to inhibit p-STAT3 and p-STAT5 in a KIT-dependent manner (Fig. 5F). These data suggest that the increased proliferative advantage of the V558Δ;V653A double mutant is intrinsic to the addition of the second-site mutation, not via increased KIT phosphorylation or activation of MAPK or PI3K pathways, but rather via KIT-dependent activation of STAT signaling.

Discussion

We established an inducible model combining a common *Kit* exon 11 (V558Δ) mutation in GIST with the most common second-site mutation (V653A), both on the same allele. It has been proposed that GIST arises from ETV1-expressing ICCs[17]. Accordingly, *Etv1* knockout mice crossed to $Kit^{V558\Delta/+}$ mice did not develop GIST[18]. Here, we demonstrated that a germline *Kit* mutation is not required for tumorigenesis in mice, and that inducing an activating *Kit* mutation in only ETV1-expressing cells after birth is sufficient for GIST development.

Notably, tumor size in germline $Kit^{V558\Delta/+}$ mice was significantly larger[14] than in the ETV1-specific mice carrying the $Kit^{V558\Delta}$ allele (not shown), possibly due to decreased efficiency of tamoxifen induction leading to a smaller proportion of cells containing the activating *Kit* mutation. In addition, it has been previously shown that the onset of ICC hyperplasia occurs prior to birth in germline $Kit^{V558\Delta/+}$ mice[25], which suggests earlier oncogenic transformation and activation in germline mutants. The ICC network, which is thought to be dependent on KIT expression[33, 34], becomes differentiated during E14–18 of murine embryogenesis[35]. Therefore, the germline mice contain an activating *Kit* mutation during a critical time in ICC differentiation which results in prenatal ICC hyperplasia, compared to the inducible mouse in which the introduction of an activating *Kit* mutation occurs postnatally in presumed non-hyperplastic ICCs.

We found that the germline $Kit^{V558\Delta;V653A}$ mutation conferred perinatal lethality. KIT signaling is important in the regulation of the hematopoietic lineage, with increased activation resulting in mastocytosis and erythrocytosis[23, 36, 37]. Because mice crossed to vav-Cre also exhibited perinatal lethality and newborns similarly displayed a red phenotype,

this suggested that death was due to effects of the V558Δ;V653A mutation in the hematopoietic lineage.

Clinically, the V654A second-site mutation is not detected in the absence of imatinib therapy, at least by current methods. In one study, no pre-existing V654A clones were able to be identified prior to initiation of imatinib despite sensitive massive parallel sequencing techniques[38]. Why untreated GISTs do not have detectable second-site *KIT* mutations remains unanswered. Our model does not answer the question of whether the second-site V654A mutation is a pre-existing, low frequency clone or develops de novo under imatinib pressure, but the former seems more likely. While our model does not replace the importance of patient-derived xenografts in modeling GIST, it allows for the study of the tumor microenvironment and of therapeutics within the context of a competent immune environment.

V558Δ;V653A tumors had a slight response to imatinib by serial MRI. However, this appeared to be unrelated to KIT inhibition. Although a previous *in vitro* study demonstrated p-KIT inhibition at 3μM[10], we were unable to demonstrate a difference in p-KIT using high dose imatinib (90 mg/kg). There has been some suggestion clinically that patients with a *KIT* exon 13 mutation may have a partial response or stable disease with imatinib[28], despite established pharmacologic resistance of KIT to imatinib[8–10]. Similarly, in our study, we found that after 4 weeks of imatinib therapy, although there was no reduction in tumor volume, the growth rate of imatinib-treated tumors was stabilized compared to vehicle-treated tumors, which grew consistently over time. This stabilization effect is suggestive of an off-target effect of imatinib in V654A *KIT* mutant GISTs, consistent with clinical observations.

Our study demonstrated the well-established efficacy of sunitinib in the treatment of GISTs with a second-site V654A mutation[11]. Given our previous study demonstrating dramatic *in vivo* tumor inhibition with cabozantinib[15], as well as a previous report of *in vitro* inhibition of the V654A KIT mutation by cabozantinib[29], we hypothesized cabozantinib would be superior to the current standard of care treatment sunitinib in our *in vivo* V558Δ;V653A model. Our results confirmed the superior anti-tumor effects of cabozantinib in the treatment of mouse GISTs with the V653A second-site mutation. In our in vivo model of V558Δ;V653A *Kit* mutation, we confirmed the activity of cabozantinib against p-KIT and identified superior treatment effects compared to sunitinib based on greater histologic effect and reduction of Ki67. Recent clinical data from the CaboGIST study, a single-arm phase II study, demonstrated 82% disease control rate in patients who had failed imatinib and sunitinib therapy[39], suggesting a role for cabozantinib in patients who have developed resistance to sunitinib. These data support cabozantinib as a more promising strategy than the current standard of sunitinib in the treatment of V654A mutant GIST. The V558Δ;V653A mouse model of GIST should be a valuable tool in the analysis and development of new therapeutics for imatinib-resistant GIST.

The V654A single mutant has been detected in an aggressive case of mast cell leukemia[40] and is reported to increase the kinase efficiency *in vitro* more than two-fold compared to WT[41]. Others have suggested that the V654A mutation alone increases proliferation in the

presence of Kit ligand compared to wild-type *KIT*[9] and has the highest kinase activity when compared to WT, D816H, D816V, V560D, and V560D;T670I *KIT* mutants *in vitro*[41]. However, the growth differential between the V559Δ single mutant and the V559Δ;V654A double mutant has not been clearly delineated. We now prove in our model that the addition of V653A to the V558Δ *Kit* mutation resulted in larger tumors, increased proliferation, and decreased survival. It has been previously demonstrated that addition or loss of mutations in tyrosine kinase receptors can change the degree of proliferation or aggressiveness of a tumor[32, 42]. Our study begins to characterize the impact of an additional mutation not only on tumor resistance to therapy, but to intrinsic tumor oncogenesis.

The increased proliferation of the V558Δ;V653A tumors was not due to an intrinsic increase in p-KIT and conventional downstream mediators in the MAPK or PI3K pathway, but associated with activation of the STAT pathway downstream of KIT. It has also been shown that different *KIT* mutations can lead to differential STAT activation[30, 32, 43]. Additionally, previous studies have demonstrated activation of various STAT proteins in GIST, most consistently STAT3 activation[31, 44]. We therefore investigated STAT signaling downstream of KIT in our model. Additionally, STAT activation may be a result of oncogenic mislocalization of the V558Δ;V653A mutant. Compartmentalization of signaling of RTKs may lead to increased STAT signaling when the mutated receptor undergoes intracellular mislocalization[45, 46]. We demonstrated increased association of STAT3 and STAT5 with KIT in the V558Δ;V653A tumors, which suggests that the addition of the V653A mutation leads to increased STAT binding to KIT, and subsequent STAT activation. In our model, activation of STAT3 and STAT5 was achieved in a KIT-dependent manner, with inhibition of STAT signaling by sunitinib and cabozantinib but not by imatinib.

In conclusion, we have created and characterized the first genetically engineered mouse model of the most common second site mutation in GIST. We demonstrated that likely due to hematopoietic transformation, the germline *Kit* V558Δ;V653A mutation resulted in perinatal lethality, which prompted us to create an ETV1-specific inducible model of GIST. Through this, we revealed the superiority of cabozantinib over sunitinib in the treatment of V653A second-site mutant GISTs in an *in vivo* setting, as well as the increased oncogenesis conferred by the V653A *Kit* mutation via STAT activation. This model is the first *in vivo* demonstration that cell-autonomous expression of mutant KIT in the ICC lineage leads to GIST and will enable a better understanding of the biology of GISTs with the second-site V654A *KIT* mutation and aid in the development of novel therapeutics to overcome resistance to imatinib and second-generation kinase inhibitors.

Materials and Methods

Generation of mouse strains.

Using the targeting vector previously employed to generate the single-mutant $Kit^{V558\Delta/+}$ mouse[23], the V653A mutation was introduced by site-directed mutagenesis into the 3' arm for homologous recombination. The 3′ arm for the $Kit^{V558\Delta;V653A}$ allele was a 1.3-kb MluI/BsrGI-NcoI fragment across exons 12–13. The final targeting vector was sequenced completely before linearization and electroporation into 129/B6 CJ7 ES cells[47]. Screening

of BamHI-digested genomic DNA from ES cell clones by Southern blot with a 3' external probe across *Kit* exon 14 yielded two positive clones for the $Kit^{V558\Delta;V653A}$ allele, confirmed by Sanger sequencing all exons. C57BL/6J blastocyst injections of one of these clones resulted in high-grade chimeras (85–100%), which gave germline transmission of the double mutation. After crossing to C57BL/6J mice, in all agouti F1 animals heterozygous for the NEO allele, the presence of the V558Δ;V653A mutation and the integrity of both loxP sites was confirmed by sequencing. To remove the floxed NEO cassette, F1 $Kit^{V558\Delta;V653A\text{-}NEO/+}$ males were bred to B6.FVB-Tg(EIIa-cre) C5379Lmgd/J females. Long-range genotyping PCR was performed across the original intron 11 MluI site, which was replaced by a 134-bp loxP scar in the case of the targeted alleles. The integrity of the exon 11 V558Δ mutation, remaining loxP site, and exon 13 V653A mutation was confirmed by sequencing. A PCR strategy bracketing the 134-bp loxP scar was used for routine genotyping thereafter (wild-type allele, 291 bp; targeted allele, 425 bp) with the primers mKitEx11F, 5′-CATAGACCCGACGCAACTTC-3′; mKitIn11R, 5′-GGTTCCCAAATCAACAAGGC-3′. A schematic is shown in Fig. 1B.

$Kit^{V558\Delta;V653A\text{-}NEO/+}$ mice were backcrossed onto the C57BL/6J background for at least seven generations before experimental use. $Kit^{V558\Delta;V653A\text{-}NEO/+}$ mice were bred to Tg(VAV1-cre)1Graf mice (a generous gift from Thomas Graf)[48], herein abbreviated as vav-Cre. $Kit^{V558\Delta;V653A\text{-}NEO/+}$ mice were also bred to B6(Cg)-$Etv1^{tm1.1(cre/ERT2)Zjh}$/J mice, herein abbreviated as $Etv1^{Cre\text{-}ERT2/+}$, and resulting progeny, both males and females, were injected once with tamoxifen (125 μg per gram of body weight) between days 0 and 5 after birth in order to induce expression of the $Kit^{V558\Delta;V653A}$ double mutation in ETV1-expressing cells. These tamoxifen-induced mice are herein referred to as V558Δ;V653A mice. In experienced hands, tamoxifen injection leads to development of tumors in >95% of mice. For controls, $Kit^{V558\Delta\text{-}NEO/+}$ single-mutant mice were similarly bred to $Etv1^{Cre\text{-}ERT2/+}$ mice and induced with tamoxifen, herein referred to as V558Δ mice. Of note, the presence of the NEO cassette results in a hypomorphic allele and not a complete loss of function, so even without Cre-mediated excision of the NEO cassette, there is reduced expression of the mutant *Kit* allele. Age of animals was 5–6 months for treatment-related experiments. Comparison of tumor weight (Fig. 3C) was performed for V558Δ (n = 22) and V558Δ;V653A mice (n = 25). Comparison of body weight (Fig. 3C) was performed for V558Δ and V558Δ;V653A mice (n = 12 per group). All animal procedures were approved by the Institutional Animal Care and Use Committee of Memorial Sloan Kettering Cancer Center.

Drug treatments *in vivo*.

$Kit^{V558\Delta;V653A\text{-}NEO/+}$; $Etv1^{Cre\text{-}ERT2/+}$ mice induced after birth were treated with imatinib 45 mg/kg i.p. bid (n = 4 per group) or 90mg/kg i.p. (n = 4 per group) as a single dose (Novartis), sunitinib 40 mg/kg p.o. daily (n = 4 per group, Sigma), or cabozantinib 60 mg/kg p.o. daily (n = 6–7 per group, Exelixis) for the indicated durations. Mice were sacrificed 3–6 hours after the last treatment. Treatment with each drug was repeated twice.

Western blot.

Protein from snap frozen tissues was isolated as before[49]. Protein from cell pellets was isolated by pipetting in NP-40 cell lysis buffer (Life Technologies) containing 1% PMSF, incubating on ice for 30 minutes, and removing cleared lysate. Antibodies were purchased from Cell Signaling Technology (p-KIT, Y719, #3391; KIT, D13A2, #3074; p-AKT, Ser473, #4060; AKT, 11E7, #4685; p-S6, S235/236, #2211; S6, 5G10, #2217; p-ERK, T202/Y204, #4370; ERK1/2, #4695; p-STAT5, Tyr694, #9359; STAT5, D2O6Y, #94205; p-STAT3, Y705, #9145; STAT3, 79D7, #4904; p-Tyrosine, p-Tyr-1000, #8954; GAPDH, #5174).

Immunoprecipitation.

For immunoprecipitation, 50 to 100 μg of protein lysate was incubated with lysis buffer to a total volume of 60 μl. One μl of STAT3 (Cell Signaling Technology, #4904) or STAT5 (Cell Signaling Technology, #94205) or 1.2 μl of KIT antibodies (Cell Signaling Technology, #3074) were added to each tube except for the mock which did not contain antibodies. Samples were subjected to rotation overnight at 4°C. Fifteen μl of protein A/G agarose beads (Santa Cruz) or Dynabeads Protein G (Life Technologies) were added to the samples and incubated for 2 hours at 4°C. Beads were centrifuged for 1 min, the supernatant was removed and the beads were washed 3 times with lysis buffer. After the last wash, the beads were resuspended in 20 μl loading buffer, vortexed, and heated to 95°C for 10 min before loading.

Immunohistochemistry.

Immunohistochemistry (IHC) was performed as before[22]. Ki67 (Abcam, #ab15580) and RFP (Rockland, #600–401-379) staining was performed by the institutional Molecular Cytology Core using a Discovery XT system (Ventana Medical Systems, Roche). Slides were either imaged on an Axio wide-field microscope (Zeiss) or scanned with MIRAX scan (Zeiss) and analyzed with Pannoramic Viewer. Ki67 was quantified by manually counting stained nuclei in the field size as indicated. N = 7 and 9 biological replicates for the V558Δ and V558Δ;V653A groups, respectively.

Mast cell isolation.

Kit$^{V558\text{-}NEO/+}$ or *Kit*$^{V558\Delta;V653A\text{-}NEO/+}$ males were bred to B6.FVB-Tg(EIIa-cre) C5379Lmgd/J females on a B6 background (Jackson Laboratory). Spleens from perinatal mice were mashed over 70μM filters and washed with media (RPMI, sodium pyruvate, penicillin, streptomycin, MEM NEAA, L-glutamine, FBS). After vortexing at 300g, the cell pellet was resuspended in 10mL of media. This cell suspension was cultured with the addition of IL3 (20ng/mL) over a period of 6 weeks at 37°C. The presence of mast cells was confirmed by flow cytometry (>98% KIT^{+}). Proliferation was measured by culturing 2 biologic replicates of WT, V558Δ, and V558Δ;V653A mast cells in duplicate with and without IL3 (6×10^5 cells, 12-well plate) over one week, with 2 experimental replicates. Cells were counted every 2–3 days.

Flow cytometry.

Flow cytometry was performed using an LSRFortessa (BD). Mouse-specific CD117 (KIT) antibody was purchased from BD Biosciences (#564012). N = 4 and 5 biological replicates for the V558Δ and V558Δ;V653A groups, respectively.

Statistical analysis.

Unpaired two-tailed Student's *t* test was performed on datasets using Graph Pad Prism 6.0 (Graph Pad Software). A *P* value <0.05 was considered significant. Data are shown as mean ± SEM. Sample sizes were at least 3 per group in order to allow for performance of the *t* test. Experimental animals were selected based on similarity in age and sex and equal sample sizes per group, otherwise no randomization technique was used. No blinding was performed for any of the experiments. Spearman correlation was performed to evaluate tumor weight as a function of mouse age.

Supplementary Material

Refer to Web version on PubMed Central for supplementary material.

Financial support:

The investigators were supported by NIH grants R01 CA102613 and T32 CA09501, and Betsy Levine-Brown and Marc Brown (RPD); GIST Cancer Research Fund (RPD and CRA); F32 CA186534 (JQZ); P50 CA140146-01 and the Starr Cancer Consortium (CRA and PB); and R01 HL55748 and CA102774 (PB). The Flow Cytometry and Molecular Cytology Core Facilities were supported by Cancer Center Support Grant P30 CA008748.

References

1. Hirota S, Isozaki K, Moriyama Y, Hashimoto K, Nishida T, Ishiguro S et al. Gain-of-function mutations of c-kit in human gastrointestinal stromal tumors. Science 1998; 279: 577–580. [PubMed: 9438854]
2. Lorincz A, Redelman D, Horvath VJ, Bardsley MR, Chen H, Ordog T. Progenitors of interstitial cells of cajal in the postnatal murine stomach. Gastroenterology 2008; 134: 1083–1093. [PubMed: 18395089]
3. Blanke CD, Rankin C, Demetri GD, Ryan CW, von Mehren M, Benjamin RS et al. Phase III randomized, intergroup trial assessing imatinib mesylate at two dose levels in patients with unresectable or metastatic gastrointestinal stromal tumors expressing the kit receptor tyrosine kinase: S0033. J Clin Oncol 2008; 26: 626–632. [PubMed: 18235122]
4. Demetri GD, von Mehren M, Blanke CD, Van den Abbeele AD, Eisenberg B, Roberts PJ et al. Efficacy and safety of imatinib mesylate in advanced gastrointestinal stromal tumors. N Engl J Med 2002; 347: 472–480. [PubMed: 12181401]
5. Joensuu H, DeMatteo RP. The management of gastrointestinal stromal tumors: a model for targeted and multidisciplinary therapy of malignancy. Annu Rev Med 2012; 63: 247–258. [PubMed: 22017446]
6. Verweij J, Casali PG, Zalcberg J, LeCesne A, Reichardt P, Blay JY et al. Progression-free survival in gastrointestinal stromal tumours with high-dose imatinib: randomised trial. Lancet 2004; 364: 1127–1134. [PubMed: 15451219]
7. Antonescu CR, Besmer P, Guo T, Arkun K, Hom G, Koryotowski B et al. Acquired resistance to imatinib in gastrointestinal stromal tumor occurs through secondary gene mutation. Clin Cancer Res 2005; 11: 4182–4190. [PubMed: 15930355]

8. Debiec-Rychter M, Cools J, Dumez H, Sciot R, Stul M, Mentens N et al. Mechanisms of resistance to imatinib mesylate in gastrointestinal stromal tumors and activity of the PKC412 inhibitor against imatinib-resistant mutants. Gastroenterology 2005; 128: 270–279. [PubMed: 15685537]

9. Roberts KG, Odell AF, Byrnes EM, Baleato RM, Griffith R, Lyons AB et al. Resistance to c-KIT kinase inhibitors conferred by V654A mutation. Mol Cancer Ther 2007; 6: 1159–1166. [PubMed: 17363509]

10. Tamborini E, Pricl S, Negri T, Lagonigro MS, Miselli F, Greco A et al. Functional analyses and molecular modeling of two c-Kit mutations responsible for imatinib secondary resistance in GIST patients. Oncogene 2006; 25: 6140–6146. [PubMed: 16751810]

11. Prenen H, Cools J, Mentens N, Folens C, Sciot R, Schoffski P et al. Efficacy of the kinase inhibitor SU11248 against gastrointestinal stromal tumor mutants refractory to imatinib mesylate. Clin Cancer Res 2006; 12: 2622–2627. [PubMed: 16638875]

12. Heinrich MC, Maki RG, Corless CL, Antonescu CR, Harlow A, Griffith D et al. Primary and secondary kinase genotypes correlate with the biological and clinical activity of sunitinib in imatinib-resistant gastrointestinal stromal tumor. J Clin Oncol 2008; 26: 5352–5359. [PubMed: 18955458]

13. Guo T, Hajdu M, Agaram NP, Shinoda H, Veach D, Clarkson BD et al. Mechanisms of sunitinib resistance in gastrointestinal stromal tumors harboring KITAY502–3ins mutation: an in vitro mutagenesis screen for drug resistance. Clin Cancer Res 2009; 15: 6862–6870. [PubMed: 19861442]

14. Sommer G, Agosti V, Ehlers I, Rossi F, Corbacioglu S, Farkas J et al. Gastrointestinal stromal tumors in a mouse model by targeted mutation of the Kit receptor tyrosine kinase. Proc Natl Acad Sci U S A 2003; 100: 6706–6711. [PubMed: 12754375]

15. Cohen NA, Zeng S, Seifert AM, Kim TS, Sorenson EC, Greer JB et al. Pharmacological Inhibition of KIT Activates MET Signaling in Gastrointestinal Stromal Tumors. Cancer Res 2015; 75: 2061–2070. [PubMed: 25836719]

16. Kim TS, Cavnar MJ, Cohen NA, Sorenson EC, Greer JB, Seifert AM et al. Increased KIT inhibition enhances therapeutic efficacy in gastrointestinal stromal tumor. Clin Cancer Res 2014; 20: 2350–2362. [PubMed: 24583793]

17. Chi P, Chen Y, Zhang L, Guo X, Wongvipat J, Shamu T et al. ETV1 is a lineage survival factor that cooperates with KIT in gastrointestinal stromal tumours. Nature 2010; 467: 849–853. [PubMed: 20927104]

18. Ran L, Sirota I, Cao Z, Murphy D, Chen Y, Shukla S et al. Combined inhibition of MAP kinase and KIT signaling synergistically destabilizes ETV1 and suppresses GIST tumor growth. Cancer Discov 2015; 5: 304–315. [PubMed: 25572173]

19. Balachandran VP, Cavnar MJ, Zeng S, Bamboat ZM, Ocuin LM, Obaid H et al. Imatinib potentiates antitumor T cell responses in gastrointestinal stromal tumor through the inhibition of Ido. Nat Med 2011; 17: 1094–1100. [PubMed: 21873989]

20. Cavnar MJ, Zeng S, Kim TS, Sorenson EC, Ocuin LM, Balachandran VP et al. KIT oncogene inhibition drives intratumoral macrophage M2 polarization. J Exp Med 2013; 210: 2873–2886. [PubMed: 24323358]

21. Seifert AM, Zeng S, Zhang JQ, Kim TS, Cohen NA, Beckman MJ et al. PD-1/PD-L1 Blockade Enhances T-cell Activity and Antitumor Efficacy of Imatinib in Gastrointestinal Stromal Tumors. Clin Cancer Res 2017; 23: 454–465. [PubMed: 27470968]

22. Zhang JQ, Zeng S, Vitiello GA, Seifert AM, Medina BD, Beckman MJ et al. Macrophages and CD8(+) T Cells Mediate the Antitumor Efficacy of Combined CD40 Ligation and Imatinib Therapy in Gastrointestinal Stromal Tumors. Cancer Immunol Res 2018; 6: 434–447. [PubMed: 29467128]

23. Bosbach B, Deshpande S, Rossi F, Shieh JH, Sommer G, de Stanchina E et al. Imatinib resistance and microcytic erythrocytosis in a KitV558Delta;T669I/+ gatekeeper-mutant mouse model of gastrointestinal stromal tumor. Proc Natl Acad Sci U S A 2012; 109: E2276–2283. [PubMed: 22652566]

24. Georgiades P, Ogilvy S, Duval H, Licence DR, Charnock-Jones DS, Smith SK et al. VavCre transgenic mice: a tool for mutagenesis in hematopoietic and endothelial lineages. Genesis 2002; 34: 251–256. [PubMed: 12434335]
25. Kwon JG, Hwang SJ, Hennig GW, Bayguinov Y, McCann C, Chen H et al. Changes in the structure and function of ICC networks in ICC hyperplasia and gastrointestinal stromal tumors. Gastroenterology 2009; 136: 630–639. [PubMed: 19032955]
26. West RB, Corless CL, Chen X, Rubin BP, Subramanian S, Montgomery K et al. The novel marker, DOG1, is expressed ubiquitously in gastrointestinal stromal tumors irrespective of KIT or PDGFRA mutation status. Am J Pathol 2004; 165: 107–113. [PubMed: 15215166]
27. Nocka K, Tan JC, Chiu E, Chu TY, Ray P, Traktman P et al. Molecular bases of dominant negative and loss of function mutations at the murine c-kit/white spotting locus: W37, Wv, W41 and W. EMBO J 1990; 9: 1805–1813. [PubMed: 1693331]
28. Heinrich MC, Owzar K, Corless CL, Hollis D, Borden EC, Fletcher CD et al. Correlation of kinase genotype and clinical outcome in the North American Intergroup Phase III Trial of imatinib mesylate for treatment of advanced gastrointestinal stromal tumor: CALGB 150105 Study by Cancer and Leukemia Group B and Southwest Oncology Group. J Clin Oncol 2008; 26: 5360–5367. [PubMed: 18955451]
29. Zhao J, Quan H, Xu Y, Kong X, Jin L, Lou L. Flumatinib, a selective inhibitor of BCR-ABL/PDGFR/KIT, effectively overcomes drug resistance of certain KIT mutants. Cancer Sci 2014; 105: 117–125. [PubMed: 24205792]
30. Chaix A, Lopez S, Voisset E, Gros L, Dubreuil P, De Sepulveda P. Mechanisms of STAT protein activation by oncogenic KIT mutants in neoplastic mast cells. J Biol Chem 2011; 286: 5956–5966. [PubMed: 21135090]
31. Duensing A, Medeiros F, McConarty B, Joseph NE, Panigrahy D, Singer S et al. Mechanisms of oncogenic KIT signal transduction in primary gastrointestinal stromal tumors (GISTs). Oncogene 2004; 23: 3999–4006. [PubMed: 15007386]
32. Chaix A, Arcangeli ML, Lopez S, Voisset E, Yang Y, Vita M et al. KIT-D816V oncogenic activity is controlled by the juxtamembrane docking site Y568-Y570. Oncogene 2014; 33: 872–881. [PubMed: 23416972]
33. Beckett EA, Ro S, Bayguinov Y, Sanders KM, Ward SM. Kit signaling is essential for development and maintenance of interstitial cells of Cajal and electrical rhythmicity in the embryonic gastrointestinal tract. Dev Dyn 2007; 236: 60–72. [PubMed: 16937373]
34. Torihashi S, Ward SM, Sanders KM. Development of c-Kit-positive cells and the onset of electrical rhythmicity in murine small intestine. Gastroenterology 1997; 112: 144–155. [PubMed: 8978353]
35. Kluppel M, Huizinga JD, Malysz J, Bernstein A. Developmental origin and Kit-dependent development of the interstitial cells of cajal in the mammalian small intestine. Dev Dyn 1998; 211: 60–71. [PubMed: 9438424]
36. Miller CL, Rebel VI, Lemieux ME, Helgason CD, Lansdorp PM, Eaves CJ. Studies of W mutant mice provide evidence for alternate mechanisms capable of activating hematopoietic stem cells. Exp Hematol 1996; 24: 185–194. [PubMed: 8641340]
37. Yee NS, Paek I, Besmer P. Role of kit-ligand in proliferation and suppression of apoptosis in mast cells: basis for radiosensitivity of white spotting and steel mutant mice. J Exp Med 1994; 179: 1777–1787. [PubMed: 7515099]
38. Heydt C, Kumm N, Fassunke J, Kunstlinger H, Ihle MA, Scheel A et al. Massively parallel sequencing fails to detect minor resistant subclones in tissue samples prior to tyrosine kinase inhibitor therapy. BMC Cancer 2015; 15: 291. [PubMed: 25886408]
39. Schoffski P, Mir O, Kasper B, Papai Z, Blay JY, Italiano A et al. Activity and safety of the multi-target tyrosine kinase inhibitor cabozantinib in patients with metastatic gastrointestinal stromal tumour after treatment with imatinib and sunitinib: European Organisation for Research and Treatment of Cancer phase II trial 1317 ‘CaboGIST’. Eur J Cancer 2020; 134: 62–74. [PubMed: 32470848]
40. Spector MS, Iossifov I, Kritharis A, He C, Kolitz JE, Lowe SW et al. Mast-cell leukemia exome sequencing reveals a mutation in the IgE mast-cell receptor beta chain and KIT V654A. Leukemia 2012; 26: 1422–1425. [PubMed: 22173243]

41. Gajiwala KS, Wu JC, Christensen J, Deshmukh GD, Diehl W, DiNitto JP et al. KIT kinase mutants show unique mechanisms of drug resistance to imatinib and sunitinib in gastrointestinal stromal tumor patients. Proc Natl Acad Sci U S A 2009; 106: 1542–1547. [PubMed: 19164557]

42. Regales L, Balak MN, Gong Y, Politi K, Sawai A, Le C et al. Development of new mouse lung tumor models expressing EGFR T790M mutants associated with clinical resistance to kinase inhibitors. PLoS One 2007; 2: e810. [PubMed: 17726540]

43. Casteran N, De Sepulveda P, Beslu N, Aoubala M, Letard S, Lecocq E et al. Signal transduction by several KIT juxtamembrane domain mutations. Oncogene 2003; 22: 4710–4722. [PubMed: 12879016]

44. Zhu MJ, Ou WB, Fletcher CD, Cohen PS, Demetri GD, Fletcher JA. KIT oncoprotein interactions in gastrointestinal stromal tumors: therapeutic relevance. Oncogene 2007; 26: 6386–6395. [PubMed: 17452978]

45. Choudhary C, Olsen JV, Brandts C, Cox J, Reddy PN, Bohmer FD et al. Mislocalized activation of oncogenic RTKs switches downstream signaling outcomes. Mol Cell 2009; 36: 326–339. [PubMed: 19854140]

46. Bahlawane C, Eulenfeld R, Wiesinger MY, Wang J, Muller A, Girod A et al. Constitutive activation of oncogenic PDGFRalpha-mutant proteins occurring in GIST patients induces receptor mislocalisation and alters PDGFRalpha signalling characteristics. Cell Commun Signal 2015; 13: 21. [PubMed: 25880691]

47. Swiatek PJ, Gridley T. Perinatal lethality and defects in hindbrain development in mice homozygous for a targeted mutation of the zinc finger gene Krox20. Genes Dev 1993; 7: 2071–2084. [PubMed: 8224839]

48. Stadtfeld M, Graf T. Assessing the role of hematopoietic plasticity for endothelial and hepatocyte development by non-invasive lineage tracing. Development 2005; 132: 203–213. [PubMed: 15576407]

49. Bosbach B, Rossi F, Yozgat Y, Loo J, Zhang JQ, Berrozpe G et al. Direct engagement of the PI3K pathway by mutant KIT dominates oncogenic signaling in gastrointestinal stromal tumor. Proc Natl Acad Sci U S A 2017; 114: E8448–E8457. [PubMed: 28923937]

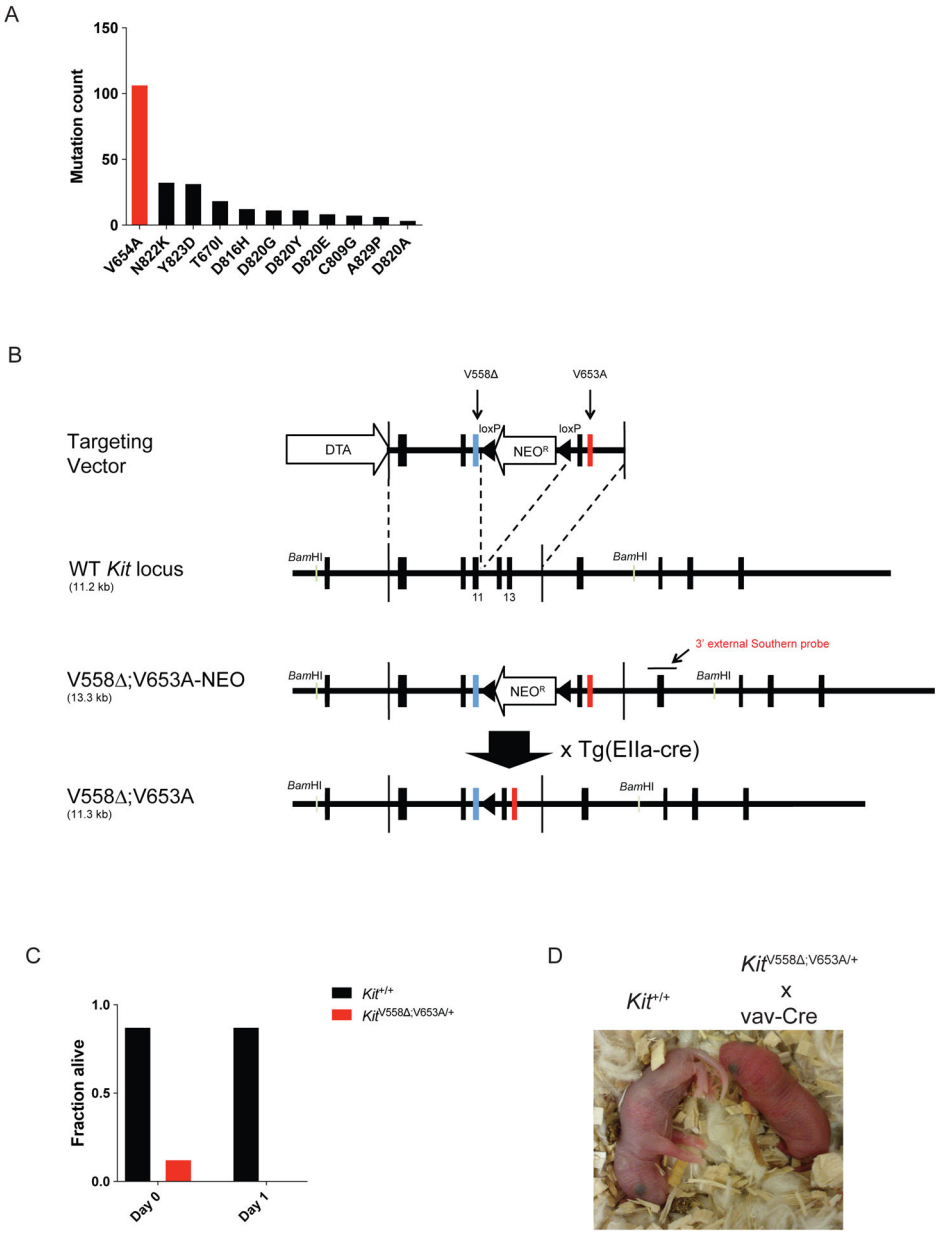

Figure 1. Germline *Kit*$^{V558\Delta;V653A/+}$ mice exhibit perinatal lethality.

(A) Incidence of V654A second-site mutations in human GIST, extracted from the COSMIC database (accessed on 3/3/2020). **(B)** Schematic representation of the knock-in mouse model containing the V558Δ and V653A mutations. **(C)** *Kit*$^{V558\Delta;V653A\text{-}NEO/+}$ mice were crossed to EIIa-cre mice and progeny (n = 32) from a total of 6 litters were counted at days 0 and 1. Fraction alive represents number of pups alive / total number of pups born. **(D)** Photo of WT mice and *Kit*$^{V558\Delta;V653A\text{-}NEO/+}$;vav-Cre mice at day 0.

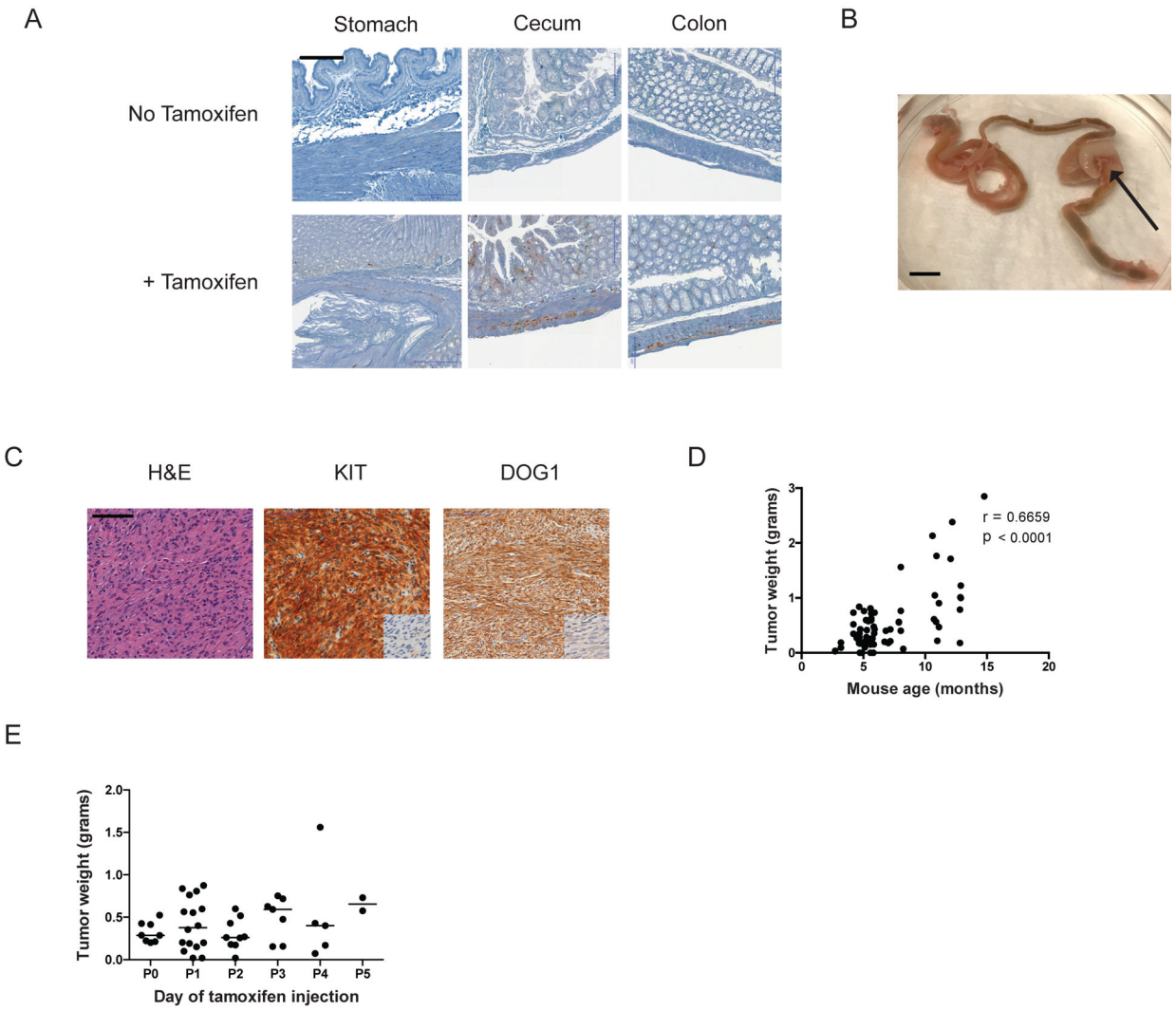

Figure 2. Inducible lineage-specific *Kit*$^{V558\Delta;V653A\text{-}NEO/+}$; *Etv1*$^{Cre\text{-}ERT2/+}$ mice develop intestinal GIST.

(A) Red fluorescent protein (RFP) IHC of cecum, colon, and stomach from *Rosa26*$^{floxSTOP\text{-}tdTomato}$ and *Rosa26*$^{floxSTOP\text{-}tdTomato}$; *Etv1*$^{Cre\text{-}ERT2/+}$ mice injected at birth with tamoxifen and sacrificed after 8 weeks of age. Staining corresponds to the region of ICCs. Bar represents 50 μm. **(B)** Representative photo of a cecal GIST in a *Kit*$^{V558\Delta;V653A\text{-}NEO/+}$; *Etv1*$^{Cre\text{-}ERT2/+}$ mouse induced with tamoxifen at birth (age 6 mo). Bar represents 1 cm. **(C)** Representative H&E as well as KIT and DOG1 IHC of a GIST from a *Kit*$^{V558\Delta;V653A\text{-}NEO/+}$; *Etv1*$^{Cre\text{-}ERT2/+}$ mouse induced with tamoxifen at birth. Isotype staining embedded right lower corner. Bar represents 100 μm. **(D)** Tumor weight of GISTs from *Kit*$^{V558\Delta;V653A\text{-}NEO/+}$; *Etv1*$^{Cre\text{-}ERT2/+}$ mice induced at birth as a function of age in months (Spearman correlation). After mice were sacrificed, tumors were resected and measured on a digital scale. **(E)** Tumor weight at 5 months of age as a function of post-natal tamoxifen injection day.

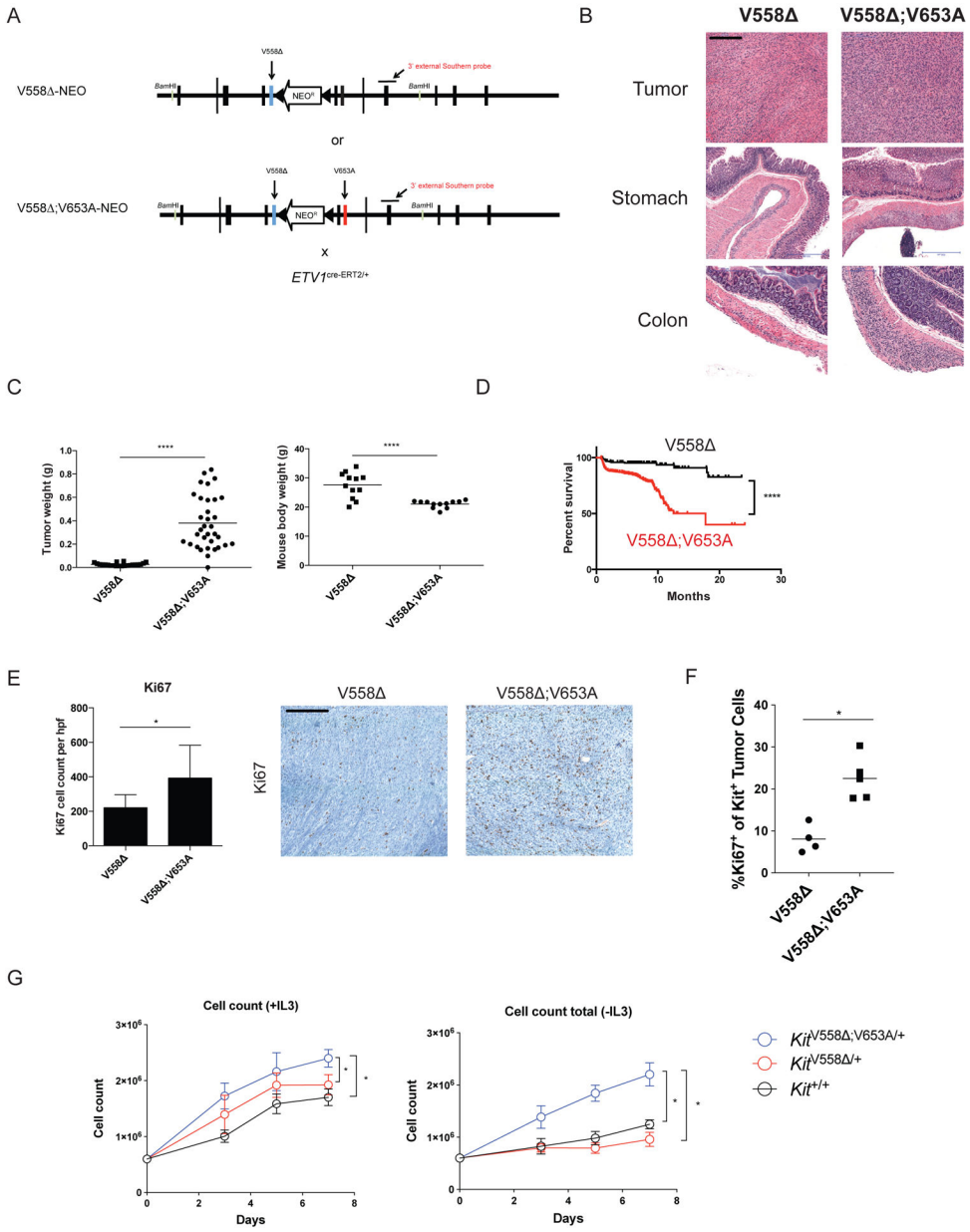

Figure 3. The V653A second-site mutation leads to increased oncogenesis compared to the V558Δ single mutation.

(**A**) Schematic of single mutant *Kit*$^{V558\Delta\text{-neo}/+}$; *Etv1*$^{Cre\text{-}ERT2/+}$ mice, used as controls for *Kit*$^{V558\Delta;V653A\text{-}NEO/+}$; *Etv1*$^{Cre\text{-}ERT2/+}$ mice harboring an additional second-site V653A mutation. Untreated single mutant *Kit*$^{V558\Delta\text{-neo}/+}$; *Etv1*$^{Cre\text{-}ERT2/+}$ mice and double mutant *Kit*$^{V558\Delta;V653A\text{-}NEO/+}$; *Etv1*$^{Cre\text{-}ERT2/+}$ mice were induced with tamoxifen at birth and sacrificed in adulthood. **(B)** H&E of tumors, stomach, and colon from untreated mice. Bar represents 200 μm for tumor and colon, and 500 μm for stomach. Untreated mice were examined for **(C)** tumor weight (5mo, n = 22–25 mice per group, left) and body weight (5mo, n = 12 mice per group, right), and **(D)** survival. **(E)** Quantitation of Ki67 IHC representing the number of positively stained nuclei in one 800 × 750 μm field (n = 7–9 mice per group) and **(F)** flow cytometry of KIT^{+} tumor cells (n = 4–5 mice per group). **(G)**

Mast cells derived from WT, *Kit*$^{V558\Delta/+}$ and *Kit*$^{V558\Delta;V653A/+}$ mice in the perinatal period were grown with and without IL3 (4 replicates each). *Kit*$^{V558\Delta\text{-neo}/+}$; *Etv1*$^{Cre\text{-}ERT2/+}$ mice induced at birth are abbreviated as V558Δ and *Kit*$^{V558\Delta;V653A\text{-}NEO/+}$; *Etv1*$^{Cre\text{-}ERT2/+}$ mice induced at birth as V558Δ;V653A. Mean ± SEM, $*P < 0.05$ using Student's *t* test.

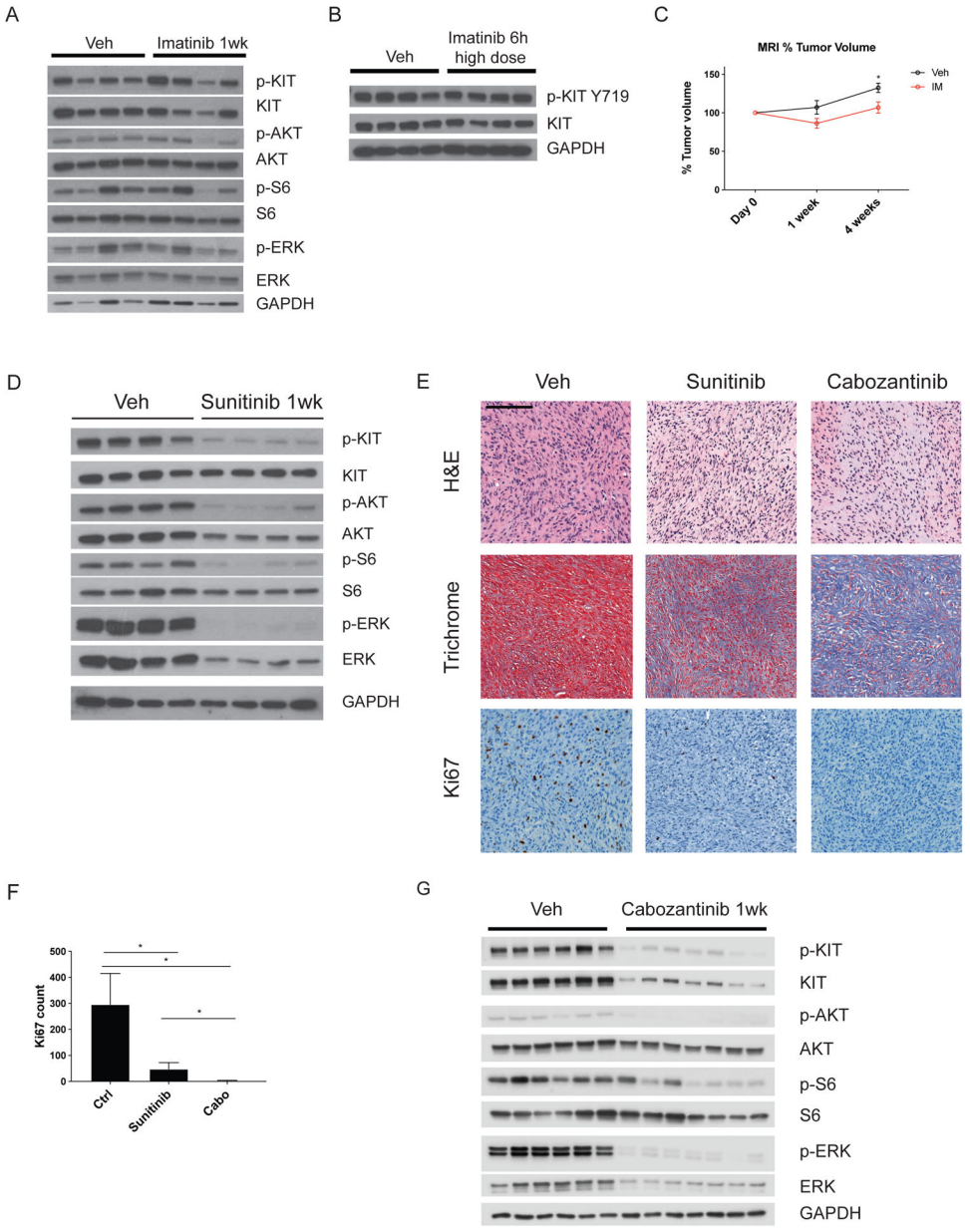

Figure 4. Cabozantinib has improved efficacy over sunitinib in imatinib-resistant GISTs from *Kit*$^{V558\Delta;V653A\text{-}NEO/+}$; *Etv1*$^{Cre\text{-}ERT2/+}$ mice.

Kit$^{V558\Delta;V653A\text{-}NEO/+}$; *Etv1*$^{Cre\text{-}ERT2/+}$ mice were induced at birth with tamoxifen and treated around 6 months of age with the indicated inhibitors. Western blot was performed after treatment with imatinib for **(A)** 1 week (45 mg/kg i.p.) and **(B)** 6 hours (90mg/kg i.p.). Mice were treated with control or imatinib for 4 weeks (n = 3–5 mice per group). **(C)** Tumor volume was measured by MRI and percent tumor volume change relative to day 0 volume was calculated at 1 and 4 weeks. Mean ± SEM, $*P < 0.05$ using Student's *t* test. **(D)** Western blot of tumors harvested after treatment with sunitinib for 1 week. **(E)** H&E, trichrome, and Ki67 IHC of tumors harvested after one week of sunitinib or cabozantinib treatment (n = 6–8 mice). Bar represents 100 μm. **(F)** Quantitation of Ki67 IHC representing the number of

positively stained nuclei in one 800 × 750 μm field. **(G)** Western blot of tumors harvested after treatment with cabozantinib for 1 week. Mean ± SEM, $*P < 0.05$ using Student's *t* test.

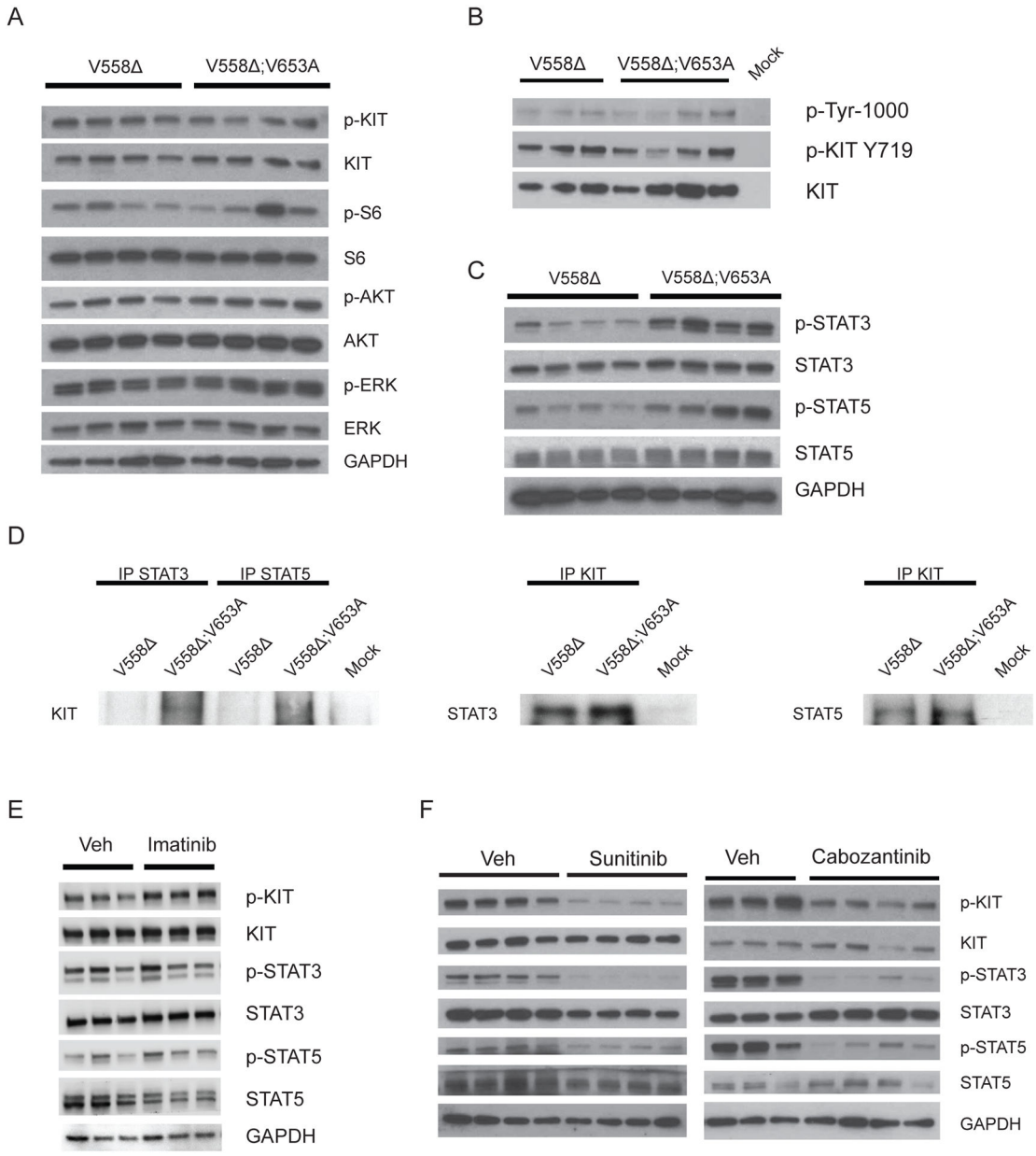

Figure 5. The V653A second-site mutation increases KIT-dependent STAT signaling.

GISTs from untreated single mutant *Kit*$^{V558\Delta\text{-neo}/+}$; *Etv1*$^{Cre\text{-}ERT2/+}$ mice and double mutant *Kit*$^{V558\Delta;V653A\text{-}NEO/+}$; *Etv1*$^{Cre\text{-}ERT2/+}$ mice induced with tamoxifen at birth and sacrificed in adulthood were analyzed by **(A, C)** western blot, **(B)** western blot of tumor lysates after immunoprecipitation with KIT antibody, and **(D)** western blot of tumor lysates after immunoprecipitation with STAT3 and STAT5 antibody (left) and KIT antibody (center and right). **(E)** Western blot of tumors from *Kit*$^{V558\Delta;V653A\text{-}NEO/+}$; *Etv1*$^{Cre\text{-}ERT2/+}$ mice induced with tamoxifen at birth and treated with 1 week of imatinib, **(F)** 1 week of sunitinib (left) and 3 hours of cabozantinib (right). *Kit*$^{V558\Delta\text{-neo}/+}$; *Etv1*$^{Cre\text{-}ERT2/+}$ mice induced at birth are

abbreviated as V558Δ and *Kit*$^{V558\Delta;V653A\text{-}NEO/+}$; *Etv1*$^{Cre\text{-}ERT2/+}$ mice induced at birth as V558Δ;V653A.